

Microscopic Investigation of Fusion and Quasifission Dynamics

Liang Li^{1,*}, Xiang-Xiang Sun^{1,**}, and Lu Guo^{1,***}

¹School of Nuclear Science and Technology, University of Chinese Academy of Sciences, Beijing 100049, China

Abstract. We introduce the application of Time-Dependent Hartree-Fock (TDHF) theory to two key aspects of heavy-ion reaction dynamics for producing superheavy elements: fusion and quasi-fission (QF). For fusion reactions $^{48}\text{Ca}+^{238}\text{U}$, the capture cross sections, fusion probabilities, and evaporation-residue cross sections are calculated using the inputs from TDHF simulations, and the results are found to be in reasonable agreement with available experimental data. For the QF process of $^{48}\text{Ca}+^{249}\text{Bk}$, we show the distribution of the fragments and investigate the impact of the tensor force, significantly enhancing the role of spherical shell effects.

1 Introduction

The investigation of superheavy elements (SHEs) constitutes a prominent and active frontier in modern nuclear physics [1–3]. Up to now, SHEs up to $Z = 118$ have been produced. This was accomplished using two kinds of reactions: cold-fusion reactions, which employed ^{208}Pb and ^{209}Bi targets for elements up to $Z = 113$ [4, 5], and hot-fusion reactions, which utilized ^{48}Ca projectiles on actinide targets to produce elements from $Z = 114$ to $Z = 118$ [6–8]. Significant experimental efforts have been made to produce superheavy nuclei with $Z = 119$ and $Z = 120$ [3, 9–11], but no successful synthesis has yet been reported.

This lack of success stems chiefly from the prevalence of quasifission, a competing mechanism that overwhelmingly dominates in heavy systems and severely inhibits compound nucleus formation. This competition becomes particularly prominent for the synthesis of the SHEs, as the enormous Coulomb repulsion makes QF the dominant reaction channel. In contrast to fusion, which leads to the formation of a fully equilibrated compound nucleus (CN), the QF process involves a different trajectory. Although the colliding nuclei surpass the capture barrier, they do not amalgamate and subsequently re-separate into two fragments [12]. As a nonequilibrium mechanism, QF is characterized by several distinct features: interaction times are typically shorter than in fusion-fission, substantial mass exchange occurs, strong correlations between fragment mass and angle are observed, and a “memory” of the entrance channel properties is partially retained [13].

Conceptually, the fusion-evaporation reaction can be understood as a three-step process: (i) the capture of the projectile by the target, forming a dinuclear system; (ii) the formation of an equilibrated CN, and (iii) the de-excitation of the CN against fission. Most theoretical approaches

provide a relatively consistent description for the capture and de-excitation process [14–16]. However, the second step, the formation of the CN, remains the most significant source of theoretical uncertainty. Predictions for this stage from various models can differ by several orders of magnitude. This crucial stage governs the evolution of the dinuclear system after capture, determining whether it proceeds to form a compact, fully equilibrated CN or re-separates into two fragments via QF. Therefore, a quantitative understanding of the fusion-QF competition, which determines the CN formation probability P_{CN} , is essential for making reliable predictions of SHE synthesis cross sections.

To achieve a quantitative understanding, various theoretical models have been developed. Macroscopic ones can be parameterized to reproduce known cross-section data, but their reliance on adjustable parameters and limited treatment of dynamics challenge their predictive power for unmeasured systems. In contrast, the microscopic TDHF approach offers insights into the underlying dynamics [17–22] and has been successfully applied to many aspects of low-energy heavy-ion collisions, including fission [23–26], fusion [21, 27–31], QF [32–36] and multinucleon transfer reactions [37–40]. Although TDHF is not suitable for the full fusion-evaporation process or quantum tunneling phenomena such as sub-barrier fusion, its simulations can provide the main ingredients for coupled-channels calculations [18, 41] and diffusion processes [30, 42, 43].

In this contribution, we introduce the results from Ref. [42] regarding the calculation of evaporation cross sections of the hot fusion reaction $^{48}\text{Ca} + ^{238}\text{U}$, where the TDHF simulations are used to provide the inputs for capture and fusion processes. We combine TDHF with both the coupled-channel (CC) and fusion-by-diffusion (FbD) approaches to calculate the cross sections of the three-step in fusion reactions. In parallel, we also show the quasifission process of $^{48}\text{Ca} + ^{249}\text{Bk}$ from Ref. [34] via TDHF

*e-mail: liliang183@mails.ucas.ac.cn

**e-mail: x.sun@fz-juelich.de

***e-mail: guolu@ucas.ac.cn

calculations, incorporating the orientation effects of deformed reactants. By analyzing the resulting fragment yield distributions with different Skyrme forces, we aim to extract the specific influence of the tensor force on the QF fragments.

2 Theoretical Framework

In the TDHF theory, the dynamic process is described by the evolution of the one-body density $\hat{\rho}$, which is obtained by solving the TDHF equation

$$i\hbar \frac{\partial}{\partial t} \hat{\rho} = [\hat{H}(\hat{\rho}), \hat{\rho}] \quad (1)$$

where \hat{H} represents the single-particle Hamiltonian derived from the effective interaction. The TDHF theory describes the collective motion semiclassically, omitting the quantum tunneling of the many-body wave function. Consequently, when calculating capture cross sections, a common and effective approach is to use internuclear potentials derived from microscopic calculations such as frozen density approximation [27], density constrained TDHF (DC-TDHF) [22, 30, 44], or density constrained frozen HF (DC-FHF) [31, 42, 45], as the input of the coupled-channels code CCFULL [46] to calculate the penetration probability.

For hot-fusion reactions, the actinide target nuclei are often strongly deformed; therefore, the orientation effects must be explicitly considered. Refs. [42] utilize the DC-FHF method to calculate the internuclear potential directly as a function of the target's orientation. In the DC-FHF method, the HF calculations are performed with the constraint that the total proton p and neutron n densities are the same as those of the ground state of the projectile and target

$$\delta \left\langle H - \int d^3r \sum_{q=p,n} \lambda_q(\mathbf{r}) \left[\rho_q^p(\mathbf{r}; \theta_p) + \rho_q^t(\mathbf{r} - \mathbf{R}; \theta_T) \right] \right\rangle = 0 \quad (2)$$

where ρ^p and ρ^t are the densities of the projectile and target for a given orientation. These densities are achieved by performing Eulerian rotations of Slater determinants in a three-dimensional Cartesian system [47]. θ_p (θ_T) denotes the angle between the symmetry axis of the deformed projectile (target) and the collision axis. \mathbf{R} is the vector between the centers of mass of the projectile and target. This variation procedure results in a unique Slater determinant $\Phi(\mathbf{R})$. The internuclear potential is then given by:

$$V(\mathbf{R}; \theta_p, \theta_T) = \langle \Phi(\mathbf{R}) | H | \Phi(\mathbf{R}) \rangle (\theta_p, \theta_T) - E_p - E_T, \quad (3)$$

where E_p and E_T are the binding energies of the projectile and target, respectively.

The penetration probabilities $T_J(E_{c.m.}, \theta_T, \theta_p)$ for each partial wave J are obtained by solving the Schrödinger equation using the incoming wave boundary condition method [46]. The orientation-average cross-section is

given as

$$\sigma_{\text{cap}}(E_{c.m.}) = \int_0^1 d \cos(\theta_p) \int_0^1 d \cos(\theta_T) \times \frac{\pi}{k^2} \sum_J (2J+1) T_J(E_{c.m.}, \theta_T, \theta_p). \quad (4)$$

where $k = \sqrt{2\mu E_{c.m.}}/\hbar$ is the wave number.

The fusion probability $P_{\text{CN}}(\theta_p, \theta_T, E_{c.m.}, J)$ is calculated using the FbD model. The key input for this model, the injection point, is estimated from TDHF simulations. The fusion cross section σ_{fus} is then obtained by folding P_{CN}

$$\sigma_{\text{fus}}(E_{c.m.}) = \int_0^1 d \cos(\theta_p) \int_0^1 d \cos(\theta_T) \times \frac{\pi}{k^2} \sum_J (2J+1) T_J(E_{c.m.}, \theta_T, \theta_p) \times P_{\text{CN}}(\theta_p, \theta_T, E_{c.m.}, J) \quad (5)$$

To facilitate comparison with experimental data, the effective fusion probability P_{fus} is defined as the ratio

$$P_{\text{fus}}(E_{c.m.}) = \frac{\sigma_{\text{fus}}(E_{c.m.})}{\sigma_{\text{cap}}(E_{c.m.})} \quad (6)$$

The survival probability $W_{\text{sur}}(E_{\text{CN}}^*, x, J)$ of the CN is calculated using a statistical model [42, 48, 49] that considers the competition between x -neutron emission and fission. The final evaporation residue (ER) cross section σ_{ER} for the xn channel is

$$\sigma_{\text{ER}}(E_{c.m.}, x) = \int_0^1 d \cos(\theta_p) \int_0^1 d \cos(\theta_T) \times \frac{\pi}{k^2} \sum_J (2J+1) T_J(E_{c.m.}, \theta_T, \theta_p) \times P_{\text{CN}}(\theta_p, \theta_T, E_{c.m.}, J) W_{\text{sur}}(E_{\text{CN}}^*, x, J) \quad (7)$$

For the QF cross section or yield for a specific reaction channel, different impact parameters and orientations result in distinct yield contributions. These contributions are quantified using

$$\sigma_\lambda \propto \int_{b_{\text{min}}}^{b_{\text{max}}} b db \int_0^{\frac{\pi}{2}} d\beta \sin(\theta_T) P_b^{(\lambda)}(\theta_T), \quad (8)$$

where λ denotes a specific reaction channel, and $P_b^{(\lambda)}(\theta_T)$ is the probability corresponding to a given impact parameter b and orientation angle θ_T . This probability is either 0 or 1 for the reaction channel λ [20, 34, 36].

3 Results and Discussions

We first investigate the capture dynamics of the $^{48}\text{Ca} + ^{238}\text{U}$ system, in which the ^{238}U target is prolate-deformed. Using the DC-FHF method, we obtain the internuclear potentials for seven orientations of ^{238}U in the range $[0, \pi/2]$. The capture cross section was then computed from these potentials using the orientation-averaged formalism. As illustrated in Fig. 1(a), orientation-averaged capture cross

sections σ_{cap} (solid red line) successfully reproduce the experimental data (solid circles) [50]. Notably, the results demonstrate a significant improvement over the predictions of the empirical coupled-channels (ECC) model [51], particularly at sub-barrier energies below $E_{\text{c.m.}} \approx 190$ MeV. The plot also clearly highlights the strong dependence on the orientation of the deformed ^{238}U target. The cross section for a near-tip collision ($\theta = 9.3^\circ$, dashed line) is substantially enhanced compared to that of a near-side collision ($\theta = 83.8^\circ$, dotted line). This enhancement is a direct consequence of the significantly lower capture barrier associated with the tip orientation.

Having established the capture cross section σ_{cap} , we next compute the orientation-averaged fusion cross section σ_{fus} (black line in Fig. 1(b)). This calculation was performed using the FbD model [15]. A key methodological strength is that the sole input parameter required by the FbD model—the injection distance—was directly extracted from our microscopic TDHF simulations. From this computed σ_{fus} and the previously calculated σ_{cap} , we then derived the effective fusion probability, $P_{\text{fus}} = \sigma_{\text{fus}}/\sigma_{\text{cap}}$, which is plotted as the red line. The resulting P_{fus} values are found to be in the range of $(2 - 6) \times 10^{-4}$. Concurrently, the calculated σ_{fus} increases slowly with incident energy.

In the third and final stage of our calculation, we determine the evaporation-residue cross sections, which are presented in Fig. 1(c) for the $3n$ (black line) and $4n$ (red line) emission channels. These final cross sections are obtained by interfacing our calculated fusion cross section σ_{fus} with the survival probability W_{sur} . This W_{sur} term is computed using a statistical model that simulates the competition between fission and neutron emission during the de-excitation of the compound nucleus. The key inputs for this stage, namely the fission barriers and neutron-separation energies, were adopted from recent microscopic-macroscopic model calculations [52]. Our calculations demonstrate good agreement with the available experimental data for both channels. This overall consistency validates our comprehensive hybrid framework, which combines microscopic TDHF theory, the CCFULL calculations, the FbD model, and a statistical model as a robust and effective method for describing the complete hot-fusion reaction process.

In the study of QF dynamics, the fragment mass-angle distributions (MADs) are crucial experimental observables. These distributions provide profound insights into the reaction mechanism, particularly by revealing the role of quantum shell effects in shaping the characteristics of the fragments [53]. To theoretically derive the MADs and the corresponding fragment yield distributions via TDHF simulations, extensive TDHF calculations are imperative [20, 34, 36]. For the $^{48}\text{Ca} + ^{249}\text{Bk}$ system, as reported in Ref. [34], we systematically sampled five distinct initial orientations of the deformed ^{249}Bk target. For each orientation, the TDHF calculations are performed by considering a wide range of impact parameters b , which begins from central collisions ($b = 0$) up to grazing trajectories where elastic scattering occurs. Figure 2 provides a direct comparison between calculations with the Skyrme

interactions SLy5t [54], which includes the tensor force, and the SLy5 set [55]. The incident energy is $E_{\text{c.m.}} = 234$ MeV in the center-of-mass frame. A clear enhancement of the neutron shell effects due to the tensor force is immediately apparent. The mass-angle correlation plot [Fig. 2(a)] reveals a pronounced clustering of QF fragments from the SLy5t simulation along the $N = 126$ magic shell closure. This feature is much less distinct in the SLy5 calculation. This observation is quantified in the fragment yield distribution [Fig. 2(c)], where the SLy5t simulation exhibits a sharp peak centered precisely at $N = 126$. In contrast, the SLy5 calculation peaks at a lower value of $N \approx 122$, indicating that the $N = 126$ shell closure plays a less dominant role in the dynamics without the tensor force.

A parallel and equally significant effect is also observed for the proton. The SLy5t fragments [Fig. 2(b), blue points] are systematically concentrated closer to the $Z = 82$ magic number than their SLy5 counterparts. This is corroborated by the proton yield distribution in Fig. 2(d). The SLy5t yield peaks are near $Z = 82$, whereas the SLy5 calculation is centered at a lower $Z \approx 79$. Collectively, these results provide strong evidence that the inclusion of the tensor force significantly amplifies the influence of the $N = 126$ and $Z = 82$ shell closures, strongly driving the QF dynamics toward the production of fragments in the vicinity of the doubly-magic ^{208}Pb .

4 Summary

We have employed the microscopic TDHF theory, in conjunction with the coupled-channel and FbD models, to investigate the capture and fusion processes in the hot-fusion reaction $^{48}\text{Ca} + ^{238}\text{U}$. For this reaction, our calculated capture cross sections are in good agreement with the experimental data. Furthermore, by accounting for the survival probability of the compound nucleus using a statistical model, our calculations successfully reproduce the experimental evaporation-residue cross sections. We also explored the QF dynamics in the $^{48}\text{Ca} + ^{249}\text{Bk}$ reaction using TDHF simulations with and without the tensor force. It is revealed that the tensor force enhances the spherical shell effects. This enhancement is clearly manifested with more fragments produced near the magic $N = 126$ neutron shell and approaching $Z = 82$ proton shell.

Acknowledgement

This work has been supported by the National Natural Science Foundation of China (Grants No.12375127, No.12435008, and No.12205308), the Strategic Priority Research Program of the Chinese Academy of Sciences (Grant No.XDB34010000), the Fundamental Research Funds for the Central Universities (Grant No. E3E46302).

References

- [1] J.H. Hamilton, S. Hofmann, Yu. Ts. Oganessian, Search for Superheavy Nuclei, *Annu. Rev. Nucl. Part. Sci.* **63**, 383 (2013). [10.1146/annurev-nucl-102912-144535](https://doi.org/10.1146/annurev-nucl-102912-144535)

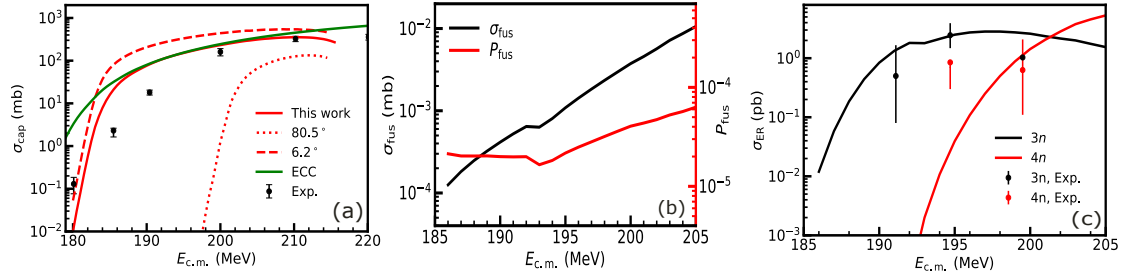


Figure 1. Theoretical results for the $^{48}\text{Ca} + ^{238}\text{U}$ reaction as a function of the center-of-mass incident energy $E_{c.m.}$. (a) Capture cross sections σ_{cap} . The orientation-averaged results (red solid line), tip ($\theta = 9.5^\circ$) and side ($\theta = 83.8^\circ$) orientations, the ECC model (green line), and experimental data (solid circles) are shown. (b) Orientation-averaged fusion cross sections σ_{fus} (black line) and effective fusion probabilities P_{fus} (red line). (c) Evaporation-residue cross sections σ_{ER} for the $3n$ (black line) and $4n$ (red line) channels, compared with experimental data (points). Taken from Ref. [42].

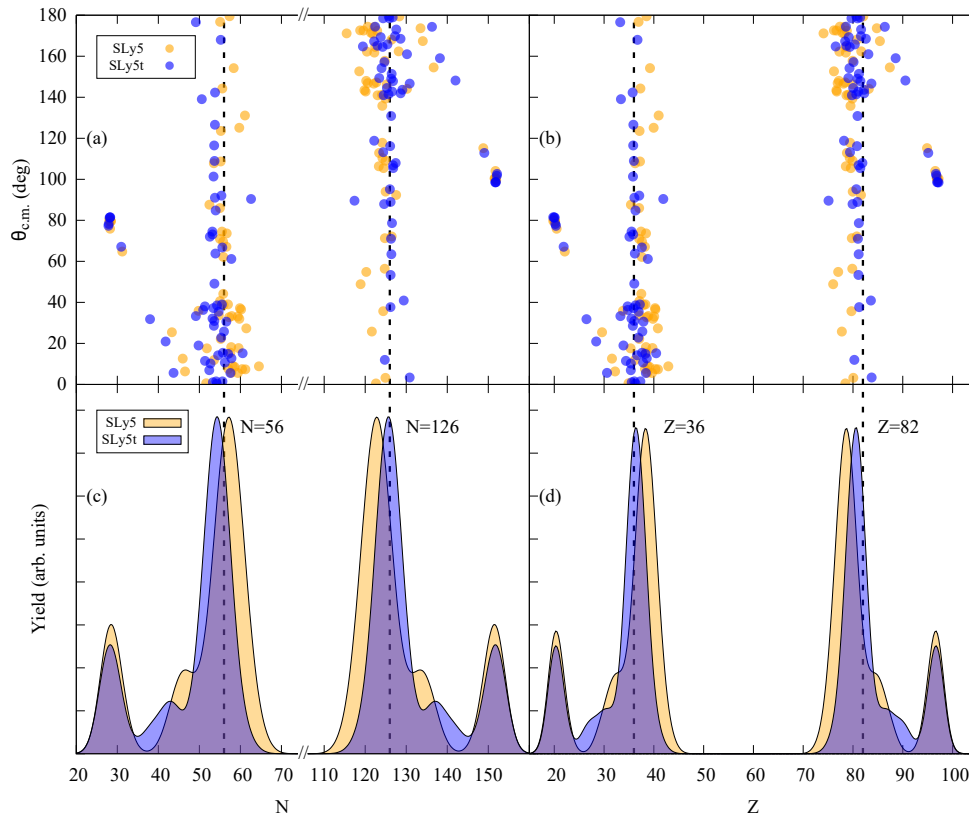


Figure 2. Quasifission reaction for the $^{48}\text{Ca} + ^{249}\text{Bk}$ at $E_{c.m.} = 234$ MeV. (a) Scattering angle $\theta_{c.m.}$ versus fragment neutron number (N). (b) $\theta_{c.m.}$ versus fragment proton number (Z). (c) Fragment neutron number yield. (d) Fragment proton number yield. In all panels, calculations including the tensor force (SLy5t, blue points/shade) are compared with those omitting it (SLy5, orange points/shade). Vertical dashed lines mark the positions of key shell closures at $N = 56, 126$ and $Z = 36, 82$. Taken from Ref. [34].

- [2] Y.T. Oganessian, V.K. Utyonkov, Super-heavy element research, **78**, 036301 (????). [10.1088/0034-4885/78/3/036301](https://doi.org/10.1088/0034-4885/78/3/036301)
- [3] S. Hofmann, S. Heinz, R. Mann, J. Maurer, G. Münzenberg, S. Antalic, W. Barth, H.G. Burkhard, L. Dahl, K. Eberhardt et al., Review of even element super-heavy nuclei and search for element 120, *Eur. Phys. J. A* **52**, 180 (2016). [10.1140/epja/i2016-16180-4](https://doi.org/10.1140/epja/i2016-16180-4)
- [4] S. Hofmann, G. Münzenberg, The discovery of the heaviest elements, *Rev. Mod. Phys.* **72**, 733 (2000).

- [10.1103/RevModPhys.72.733](https://doi.org/10.1103/RevModPhys.72.733)
- [5] K. Morita, K. Morimoto, D. Kaji, T. Akiyama, S. ichi Goto, H. Haba, E. Ideguchi, R. Kanungo, K. Katori, H. Koura et al., Experiment on the Synthesis of Element 113 in the Reaction $^{209}\text{Bi}(^{70}\text{Zn}, n)^{278}113$, *J. Phys. Soc. Japan* **73**, 2593 (2004). [10.1143/jpsj.73.2593](https://doi.org/10.1143/jpsj.73.2593)
- [6] Yu. Ts. Oganessian, V.K. Utyonkov, Yu. V. Lobanov, F. Sh. Abdullin, A.N. Polyakov, R.N. Sagaidak, I.V. Shirokovsky, Yu. S. Tsyganov, A.A. Voinov, G.G. Gulbekian et al., Synthesis of the isotopes of ele-

- ments 118 and 116 in the ^{249}Cf and $^{245}\text{Cm} + ^{48}\text{Ca}$ fusion reactions, *Phys. Rev. C* **74**, 044602 (2006). [10.1103/PhysRevC.74.044602](https://doi.org/10.1103/PhysRevC.74.044602)
- [7] Yuri Oganessian, Heaviest nuclei from ^{48}Ca -induced reactions, *J. Phys. G: Nucl. Part. Phys.* **34**, R165 (2007). [10.1088/0954-3899/34/4/R01](https://doi.org/10.1088/0954-3899/34/4/R01)
- [8] Yu. Ts. Oganessian, F. Sh. Abdullin, P.D. Bailey, D.E. Benker, M.E. Bennett, S.N. Dmitriev, J.G. Ezold, J.H. Hamilton, R.A. Henderson, M.G. Itkis et al., Synthesis of a New Element with Atomic Number $Z = 117$, *Phys. Rev. Lett.* **104**, 142502 (2010). [10.1103/PhysRevLett.104.142502](https://doi.org/10.1103/PhysRevLett.104.142502)
- [9] Y.T. Oganessian, V.K. Utyonkov, Y.V. Lobanov, F.S. Abdullin, A.N. Polyakov, R.N. Sagaidak, I.V. Shirokovsky, Y.S. Tsyganov, A.A. Voinov, A.N. Mezentsev et al., Attempt to produce element 120 in the $^{244}\text{Pu} + ^{58}\text{Fe}$ reaction, *Phys. Rev. C* **79**, 024603 (2009). [10.1103/PhysRevC.79.024603](https://doi.org/10.1103/PhysRevC.79.024603)
- [10] E.M. Kozulin, G.N. Knyazheva, I.M. Itkis, M.G. Itkis, A.A. Bogachev, L. Krupa, T.A. Loktev, S.V. Smirnov, V.I. Zagrebaev, J. Äystö et al., Investigation of the reaction $^{64}\text{Ni} + ^{238}\text{U}$ being an option of synthesizing element 120, *Phys. Lett. B* **686**, 227 (2010). [10.1016/j.physletb.2010.02.041](https://doi.org/10.1016/j.physletb.2010.02.041)
- [11] J. Khuyagbaatar, A. Yakushev, C.E. Düllmann, D. Ackermann, L.L. Andersson, M. Asai, M. Block, R.A. Boll, H. Brand, D.M. Cox et al., Search for elements 119 and 120, *Phys. Rev. C* **102**, 064602 (2020). [10.1103/PhysRevC.102.064602](https://doi.org/10.1103/PhysRevC.102.064602)
- [12] B.B. Back, R.R. Betts, K. Cassidy, B.G. Glagola, J.E. Gindler, L.E. Glendenin, B.D. Wilkins, Experimental Signatures of Quasifission Reactions, *Phys. Rev. Lett.* **50**, 818 (1983). [10.1103/PhysRevLett.50.818](https://doi.org/10.1103/PhysRevLett.50.818)
- [13] E. Vardaci, M.G. Itkis, I.M. Itkis, G. Knyazheva, E.M. Kozulin, Fission and quasifission toward the superheavy mass region, *J. Phys. G: Nucl. Part. Phys.* **46**, 103002 (2019). [10.1088/1361-6471/ab3118](https://doi.org/10.1088/1361-6471/ab3118)
- [14] N.V. Antonenko, E.A. Cherepanov, A.K. Nasirov, V.P. Permyakov, V.V. Volkov, Competition between complete fusion and quasi-fission in reactions between massive nuclei. The fusion barrier, *Phys. Lett. B* **319**, 425 (1993). [10.1016/0370-2693\(93\)91746-A](https://doi.org/10.1016/0370-2693(93)91746-A)
- [15] W.J. Świątecki, K. Siwek-Wilczyńska, J. Wilczyński, Fusion by diffusion. II. Synthesis of transfermium elements in cold fusion reactions, *Phys. Rev. C* **71**, 014602 (2005). [10.1103/PhysRevC.71.014602](https://doi.org/10.1103/PhysRevC.71.014602)
- [16] V. Zagrebaev, W. Greiner, Cross sections for the production of superheavy nuclei, *Nucl. Phys. A* **944**, 257 (2015). [10.1016/j.nuclphysa.2015.02.010](https://doi.org/10.1016/j.nuclphysa.2015.02.010)
- [17] C. Simenel, A.S. Umar, Heavy-ion collisions and fission dynamics with the time-dependent Hartree-Fock theory and its extensions, *Prog. Part. Nucl. Phys.* **103**, 19 (2018). [10.1016/j.ppnp.2018.07.002](https://doi.org/10.1016/j.ppnp.2018.07.002)
- [18] L. Guo, C. Simenel, L. Shi, C. Yu, The role of tensor force in heavy-ion fusion dynamics, *Phys. Lett. B* **782**, 401 (2018). [10.1016/j.physletb.2018.05.066](https://doi.org/10.1016/j.physletb.2018.05.066)
- [19] P.D. Stevenson, M.C. Barton, Low-energy heavy-ion reactions and the Skyrme effective interaction, *Prog. Part. Nucl. Phys.* **104**, 142 (2019). [10.1016/j.ppnp.2018.09.002](https://doi.org/10.1016/j.ppnp.2018.09.002)
- [20] K. Godbey, A.S. Umar, C. Simenel, Deformed shell effects in $^{48}\text{Ca} + ^{249}\text{Bk}$ quasifission fragments, *Phys. Rev. C* **100**, 024610 (2019). [10.1103/PhysRevC.100.024610](https://doi.org/10.1103/PhysRevC.100.024610)
- [21] X.X. Sun, L. Guo, Effects of the tensor force on low-energy heavy-ion fusion reactions: A mini review, *Commun. Theor. Phys.* **74**, 097302 (2022). [10.1088/1572-9494/ac7e28](https://doi.org/10.1088/1572-9494/ac7e28)
- [22] L. Guo, K. Godbey, A.S. Umar, Influence of the tensor force on the microscopic heavy-ion interaction potential, *Phys. Rev. C* **98**, 064607 (2018). [10.1103/PhysRevC.98.064607](https://doi.org/10.1103/PhysRevC.98.064607)
- [23] C. Simenel, A.S. Umar, Formation and dynamics of fission fragments, *Phys. Rev. C* **89**, 031601(R) (2014). [10.1103/PhysRevC.89.031601](https://doi.org/10.1103/PhysRevC.89.031601)
- [24] P.M. Goddard, P.D. Stevenson, A. Rios, Fission dynamics within time-dependent Hartree-Fock: deformation-induced fission, *Phys. Rev. C* **92**, 054610 (2015). [10.1103/PhysRevC.92.054610](https://doi.org/10.1103/PhysRevC.92.054610)
- [25] Y. Huang, X.X. Sun, L. Guo, Fission fragment distributions within time-dependent density functional theory, *Eur. Phys. J. A* **60**, 100 (2024). [10.1140/epja/s10050-024-01326-2](https://doi.org/10.1140/epja/s10050-024-01326-2)
- [26] Y. Huang, X.X. Sun, L. Guo, Role of the tensor force in induced fission of ^{240}Pu , *Phys. Rev. C* **110**, 064318 (2024). [10.1103/PhysRevC.110.064318](https://doi.org/10.1103/PhysRevC.110.064318)
- [27] L. Guo, T. Nakatsukasa, Time-dependent Hartree-Fock studies of the dynamical fusion threshold, *EPJ Web Conf.* **38**, 09003 (2012). [10.1051/epj-conf/20123809003](https://doi.org/10.1051/epj-conf/20123809003)
- [28] K. Washiyama, Microscopic analysis of fusion hindrance in heavy nuclear systems, *Phys. Rev. C* **91**, 064607 (2015). [10.1103/PhysRevC.91.064607](https://doi.org/10.1103/PhysRevC.91.064607)
- [29] X. Li, Z. Wu, L. Guo, Entrance-channel dynamics in the reaction $^{40}\text{Ca} + ^{208}\text{Pb}$, *Sci. China-Phys. Mech. Astron.* **62**, 122011 (2019). [10.1007/s11433-019-9435-x](https://doi.org/10.1007/s11433-019-9435-x)
- [30] X.X. Sun, L. Guo, A.S. Umar, Microscopic study of the fusion reactions $^{40,48}\text{Ca} + ^{78}\text{Ni}$ and the effect of the tensor force, *Phys. Rev. C* **105**, 034601 (2022). [10.1103/PhysRevC.105.034601](https://doi.org/10.1103/PhysRevC.105.034601)
- [31] X.X. Sun, L. Guo, Microscopic study of fusion reactions with a weakly bound nucleus: Effects of deformed halo, *Phys. Rev. C* **107**, L011601 (2023). [10.1103/PhysRevC.107.L011601](https://doi.org/10.1103/PhysRevC.107.L011601)
- [32] C. Yu, L. Guo, Angular momentum dependence of quasifission dynamics in the reaction $^{48}\text{Ca} + ^{244}\text{Pu}$, *Sci. China-Phys. Mech. Astron.* **60**, 092011 (2017). [10.1007/s11433-017-9063-3](https://doi.org/10.1007/s11433-017-9063-3)
- [33] L. Guo, C. Shen, C. Yu, Z. Wu, Isotopic trends of quasifission and fusion-fission in the reactions $^{48}\text{Ca} + ^{239,244}\text{Pu}$, *Phys. Rev. C* **98**, 064609 (2018). [10.1103/PhysRevC.98.064609](https://doi.org/10.1103/PhysRevC.98.064609)
- [34] L. Li, L. Guo, K. Godbey, A.S. Umar, Impact of tensor force on quantum shell effects in quasifission reactions, *Phys. Lett. B* **833**, 137349 (2022).

- 10.1016/j.physletb.2022.137349
- [35] H. Lee, P. McGlynn, C. Simenel, Shell effects in quasifission in reactions forming the ^{226}Th compound nucleus, *Phys. Rev. C* **110**, 024606 (2024). [10.1103/PhysRevC.110.024606](https://doi.org/10.1103/PhysRevC.110.024606)
- [36] L. Li, L. Guo, K. Godbey, A.S. Umar, Impact of tensor forces on quasifission product yield distributions, *Phys. Rev. C* **110**, 064607 (2024). [10.1103/PhysRevC.110.064607](https://doi.org/10.1103/PhysRevC.110.064607)
- [37] G.F. Dai, L. Guo, E.G. Zhao, S.G. Zhou, Dissipation dynamics and spin-orbit force in time-dependent Hartree-Fock theory, *Phys. Rev. C* **90**, 044609 (2014). [10.1103/PhysRevC.90.044609](https://doi.org/10.1103/PhysRevC.90.044609)
- [38] Z. Wu, L. Guo, Microscopic studies of production cross sections in multinucleon transfer reaction $^{58}\text{Ni} + ^{124}\text{Sn}$, *Phys. Rev. C* **100**, 014612 (2019). [10.1103/PhysRevC.100.014612](https://doi.org/10.1103/PhysRevC.100.014612)
- [39] K. Sekizawa, S. Ayik, Quantal diffusion approach for multinucleon transfer processes in the $^{58,64}\text{Ni} + ^{208}\text{Pb}$ reactions: Toward the production of unknown neutron-rich nuclei, *Phys. Rev. C* **102**, 014620 (2020). [10.1103/PhysRevC.102.014620](https://doi.org/10.1103/PhysRevC.102.014620)
- [40] Z. Wu, L. Guo, Z. Liu, G. Peng, Production of proton-rich nuclei in the vicinity of ^{100}Sn via multinucleon transfer reactions, *Phys. Lett. B* **825**, 136886 (2022). [10.1016/j.physletb.2022.136886](https://doi.org/10.1016/j.physletb.2022.136886)
- [41] N. Wang, X. Wu, Z. Li, M. Liu, W. Scheid, Applications of Skyrme energy-density functional to fusion reactions for synthesis of superheavy nuclei, *Phys. Rev. C* **74**, 044604 (2006). [10.1103/PhysRevC.74.044604](https://doi.org/10.1103/PhysRevC.74.044604)
- [42] X.X. Sun, L. Guo, Microscopic study of the hot-fusion reaction $^{48}\text{Ca} + ^{238}\text{U}$ with the constraints from time-dependent Hartree-Fock theory, *Phys. Rev. C* **107**, 064609 (2023). [10.1103/PhysRevC.107.064609](https://doi.org/10.1103/PhysRevC.107.064609)
- [43] K. Sekizawa, K. Hagino, Time-dependent Hartree-Fock plus Langevin approach for hot fusion reactions to synthesize the $Z = 120$ superheavy element, *Phys. Rev. C* **99**, 051602(R) (2019). [10.1103/PhysRevC.99.051602](https://doi.org/10.1103/PhysRevC.99.051602)
- [44] K. Godbey, L. Guo, A.S. Umar, Influence of the tensor interaction on heavy-ion fusion cross sections, *Phys. Rev. C* **100**, 054612 (2019). [10.1103/PhysRevC.100.054612](https://doi.org/10.1103/PhysRevC.100.054612)
- [45] C. Simenel, A.S. Umar, K. Godbey, M. Dasgupta, D.J. Hinde, How the Pauli exclusion principle affects fusion of atomic nuclei, *Phys. Rev. C* **95**, 031601(R) (2017). [10.1103/PhysRevC.95.031601](https://doi.org/10.1103/PhysRevC.95.031601)
- [46] K. Hagino, N. Rowley, A.T. Kruppa, A program for coupled-channel calculations with all order couplings for heavy-ion fusion reactions, *Comput. Phys. Commun.* **123**, 143 (1999). [10.1016/s0010-4655\(99\)00243-x](https://doi.org/10.1016/s0010-4655(99)00243-x)
- [47] D.A. Pigg, A.S. Umar, V.E. Oberacker, Eulerian rotations of deformed nuclei for TDDFT calculations, *Comput. Phys. Commun.* **185**, 1410 (2014). [10.1016/j.cpc.2014.02.004](https://doi.org/10.1016/j.cpc.2014.02.004)
- [48] N. Bohr, J.A. Wheeler, The Mechanism of Nuclear Fission, *Phys. Rev.* **56**, 426 (1939). [10.1103/physrev.56.426](https://doi.org/10.1103/physrev.56.426)
- [49] Z.Q. Feng, G.M. Jin, F. Fu, J.Q. Li, Production cross sections of superheavy nuclei based on dinuclear system model, *Nucl. Phys. A* **771**, 50 (2006). [10.1016/j.nuclphysa.2006.03.002](https://doi.org/10.1016/j.nuclphysa.2006.03.002)
- [50] K. Nishio, S. Mitsuoka, I. Nishinaka, H. Makii, Y. Wakabayashi, H. Ikezoe, K. Hirose, T. Ohtsuki, Y. Aritomo, S. Hofmann, Fusion probabilities in the reactions $^{40,48}\text{Ca} + ^{238}\text{U}$ at energies around the Coulomb barrier, *Phys. Rev. C* **86**, 034608 (2012). [10.1103/PhysRevC.86.034608](https://doi.org/10.1103/PhysRevC.86.034608)
- [51] B. Wang, K. Wen, W.J. Zhao, E.G. Zhao, S.G. Zhou, Systematics of capture and fusion dynamics in heavy-ion collisions, *At. Data Nucl. Data Tables* **114**, 281 (2017). [10.1016/j.adt.2016.06.003](https://doi.org/10.1016/j.adt.2016.06.003)
- [52] P. Jachimowicz, M. Kowal, J. Skalski, Properties of heaviest nuclei with $98 \leq Z \leq 126$ and $134 \leq N \leq 192$, *Atomic Data and Nuclear Data Tables* **138**, 101393 (2021). [10.1016/j.adt.2020.101393](https://doi.org/10.1016/j.adt.2020.101393)
- [53] A. Wakhle, C. Simenel, D.J. Hinde, M. Dasgupta, M. Evers, D.H. Luong, R. du Rietz, E. Williams, Interplay between Quantum Shells and Orientation in Quasifission, *Phys. Rev. Lett.* **113**, 182502 (2014). [10.1103/PhysRevLett.113.182502](https://doi.org/10.1103/PhysRevLett.113.182502)
- [54] G. Colò, H. Sagawa, S. Fracasso, P.F. Bortignon, Spin-orbit splitting and the tensor component of the Skyrme interaction, *Phys. Lett. B* **646**, 227 (2007). [10.1016/j.physletb.2007.01.033](https://doi.org/10.1016/j.physletb.2007.01.033)
- [55] E. Chabanat, P. Bonche, P. Haensel, J. Meyer, R. Schaeffer, A Skyrme parametrization from subnuclear to neutron star densities Part II. Nuclei far from stabilities, *Nucl. Phys. A* **635**, 231 (1998). [10.1016/S0375-9474\(98\)00180-8](https://doi.org/10.1016/S0375-9474(98)00180-8)